韓國水資源學會論文集
第33卷 第2號 · 2000年 4月
pp. 181 ~ 193

# 파랑존재시 해저 모래결위의 부유사 농도분포

## Suspended Sediment Concentrations over Ripples for Waves

김 효 섭* / 김 태 형**
Kim, Hyo Seob / Kim, Tae Hyung

### Abstract

This paper presents the flow and the suspended sediment movement over ripples for oscillatory flows. A new numerical model system is developed, and applied to a laboratory experimental condition of regular waves and a ficticious condition of irregular waves. The flow field is obtained from a programme proposed by Kim *et al.*(1994), which is a modified version of SOLA based on SMAC scheme. The sub-model solves the continuity and Reynolds momentum equations in the x-z plane. The wave orbital velocities, shear stresses, and pressure are all reasonably reproduced by the model. The model results on the vertical velocity component show good agreement with the measurements. The suspended sediment transport sub-model is newly set up to solve the advection-diffusion equation of suspended sediment using a split method, and involving a special shear entrainment from the whole ripple surface. The calculated suspended sediment concentrations for regular waves show reasonable agreement with measurements at Deltaflume. The model results for random waves show that the suspended sediment concentration is higher than those for regular waves and that the sediment diffuses higher than for regular waves with the significant wave height and the peak wave period of the irregular waves.
*Keywords*: suspended sediment concentration, wave, numerical model

### 요 지

본 논문에서는 파랑이 존재할 때 모래결위에서의 흐름과 부유사의 거동에 관하여 기술한다. 새로운 수치모형시스템을 구축하였으며 이를 규칙파랑을 이용한 기존 실험실 실험조건과 가상적불규칙파랑조건에 적용하였다. 흐름장 계산은 SMAC 방법에 근거한 프로그램 SOLA를 Kim 등(1994)이 일부 수정하여 제시한 프로그램을 사용하였다. 흐름계산 부모형은 x-z 면에서의 연속방정식과 Reynolds의 운동방정식을 기본방정식으로 한다. 흐름부모형으로 파랑궤적속도, 전단응력, 압력의 분포를 계산하였다. 모형실험결과 중 수직방향궤적속도는 관측자료와 잘 일치하였다. 퇴적물이동 부모형은 부유사의 이류확산을 나타내는 식을 기본방정식으로 한다. 수치기법은 분리기법을 이용하며, 모래결 표면으로부터 퇴적물이 연행되어 유체내로 투입된다. 규칙파랑 실험조건에 수치모형을 적용한 결과, 부유사농도의 연직분포가 Deltaflume의 실험자료와 유사하게 재현되었다. 가상적인 불규칙 파랑조건에 모형을 적용한 결과 부유사농도가 높게, 부유사확산 범위가 더 넓게 예측되었다.
**핵심용어** : 부유사농도, 파랑, 수치모형

* 국민대학교 공과대학 토목 · 환경공학부 조교수
Assistant Prof., School of Civil & Environmental Engineering Kookmin University, Seoul, 136-701, Korea
(hkim@kmu.kookmin.ac.kr)
** 국민대학교 대학원 토목공학과 석사과정
Graduate Student, Department of Civil & Environmental Engineering Kookmin University, Seoul, 136-701, Korea

## 1. INTRODUCTION

Short or medium-term coastal morphological changes over the world have been studied for the engineering purposes. Morphological change and sediment transport are closely linked to the micro-scale seabed forms. The mechanism of ripple growth or transition between rippled beds and flat beds has not yet been completely understood. Previous works on the movement of suspended sediment over ripples include field measurements, laboratory experiments, and numerical modelling works.

Laboratory experimental works of flow or sediment transport over ripples include Bosman(1982), and Williams *et al.*(1998). The experiments have been carried out at oscillating tray rigs, oscillating water tunnels, or wave flumes.

Several numerical models have been proposed to describe flows or suspended sediment concentrations over ripples up to the present. Existing modelling works of flow over ripples include Du Toit and Sleath(1981), Longuet-Higgins(1981), Sato(1987), Huynh-Thanh and Temperville(1990), Blondeaux and Vittori(1990), Hansen et al.(1991), and Kim *et al.*(1994).

Longuet-Higgins(1981) proposed a discrete vortex method with the conformal transformation to reproduce the flow over sharp-crested ripples. The calculated drag coefficients were compared to Bagnold's(1946) experimental results, and gave good agreement.

Kim *et al.*(1994) used a marker-and-cell (MAC) method to calculate the flow over ripples. They set up a computational grid in the 2DV (x-z) domain and expressed the ripple surface by small rectangular grids. They examined the effect of wave asymmetry on the flow characteristics, e.g. velocity, vorticity, shear stress, and turbulence energy. Their calculation results gave good agreement with measured velocities, vorticities, turbulence energy, and eddy viscosity. They also predicted the effect of second harmonics of wave orbital velocities on the vorticity over ripples.

Du Toit and Sleath(1981) compared their laboratory experimental results and Sleath's numerical model results on the flow over ripples. Even though Sleath's model adopted laminar viscosity for the turbulent flow condition, his model showed close agreement with measurements.

Previous modelling works on sediment transport over ripples include Sato(1987), Huynh-Thanh and Temperville(1990), Blondeaux and Vittori(1990), O'Connor et al.(1992), and O'Connor(1998).

Sato(1987) used a random walk approach to represent the diffusion process of the suspended sediment concentration. He obtained the suspended sediment concentration by counting the number of sediment particles. However, Sato has not verified his model results with measurements.

Blondeaux and Vittori(1990) performed laboratory and numerical experiments on the sediment motion over a rippled bed. They presented good qualitative agreements between visualization results and the random walk numerical model results.

Hansen et al.(1991) adopted a random walk approach for description of sediment transport following a discrete vortex flow model. They assumed that the entained sediment particles are released at a point over the ripple crest. Their model results were not accurate for the large Shields parameter cases.

Tsujimoto et al.(1991) carried out laboratory and numerical experiments on the sediment transport over ripples using a k-equation turbulence model. However, their solution depends largely on the bed boundary condition for the sediment concentration.

O'Connor(1998) has started to solve the advection-diffusion equation using a finite

difference method, and has shown reasonable test results.

Sediment transport has usually been calculated by separate sediment transport models making use of the flow model results. Existing sediment transport models can be classified into two groups, the random walk method, and the finite difference or element method.

Sato(1987), MacPherson(1989), Tsujimoto et al.(1991), and Hansen et al.(1991) have used the random walk method with many individual sediment particles, while O'Connor(1998) has solved the advection-diffusion equation using a finite difference method in the 2DV domain.

The former approach describes the diffusion due to turbulence as random movement of sediment particles with a distance having a corresponding variance at every calculation space and time. At the bottom boundary, sediment particles are simply got rid of, when they hit the bed boundary.

In contrast to the random walk approach, the governing advection-diffusion equation can be directly solved using a finite difference method, which does not involve the random movement of sediment particles. The advection-diffusion model should properly treat the fluid-solid bed boundary, where the sediment concentration is high, and the gradient of concentration is also high. A reasonable boundary condition at the bed boundary is the free settling condition with no diffusion, and the condition that the sediment is entrained in vortices from the bed surface and supplied to the fluid over the ripples. In both cases, the description of entrainment or pick up of bed sediment takes an important role in the model.

Sediment entrainment has been described in several different ways by researchers. Typical empirical formulas for sediment entrainment rate have been proposed by MacPherson(1984) and Nielsen(1992).

MacPherson(1984) adopted an empirical formula for entrainment rate at ripple crests as follows:

$$E = \begin{cases} C_1\left(\dfrac{u^2 - u_{cri}^2}{u_\infty^2}\right)^n, & u > u_{cri} \\ 0, & u \le u_{cri} \end{cases} \quad (1)$$

where $E$ is the entrainment rate, $u$ is the local wave induced orbital velocity over the ripple crest, $u_{cri}$ is the critical orbital velocity for incipient sediment movement, $u_\infty$ is the amplitude of the wave orbital velocity variation, $n$ is the empirical parameter, and $C_1$ is the empirical coefficient.

The above equation can be reformed into the following equation:

$$E = \begin{cases} C_2(\tau - \tau_{cri})^n, & \tau > \tau_{cri} \\ 0, & \tau \le \tau_{cri} \end{cases} \quad (2)$$

where $\tau$ is the bed shear stress, and $\tau_{cri}$ is the critical shear stress for entrainment. The coefficient $C_1$ or $C_2$ can be chosen from calibration with measurements. Equation (1) can be considered as a specific form of a universal equation. MacPherson(1984) assumed that the entrained sediment is supplied at a point over the ripple crest, the height of the point from the ripple crest was also empirically decided. MacPherson's(1984) trial could explain the general behaviour of the wave-induced suspended sediment over ripples, e.g. entrainment in vortices and burst after vortex ejection. However, the sediment particles were released at just one point over the ripple crest per ripple length, so that the sediment entrainment from other places of the bed surface could not be taken into account in his model. Van Rijn(1989) proposed a general formula of sediment entrainment for wave and current. However, his formula was still based on a restricted number of data sets.

Nielsen(1992) proposed an empirical formula using delta functions to express the vortex entrainment over ripples, that is:

$$E = V_1\delta(t - t_1) + V_2\delta(t - t_2) \quad (3)$$

where $V_1$ and $V_2$ are the total amount of entrained sediment at two flow reversal events, $\delta$ is the periodic delta function, t is time, and $t_1$ and $t_1$ are the times of flow reversals. However, Nielsen(1992) has not proposed further methodology how to obtain $V_1$ and $V_2$.

Differently from the above formula, Nielsen(1992) proposed an empirical formula of entrainment over flat beds as follows:

$$E \cong \begin{cases} 0.017\omega_f(\theta - \theta_{cri})^{1.5}F, & \theta > \theta_{cri} \\ 0, & \theta \le \theta_{cri} \end{cases} \quad (4)$$

where $\theta$ is the instantaneous Shields parameter, and $\theta_{cri}$ is the critical Shields parameter for the initiation of sediment movement which is around 0.05, and $F$ is the function representing the effect of phase lag between the near-bed velocity and the bed shear stress.

The present review of the previous works suggests that it is more desirable to allow entrainment on the whole ripple surface in order to model the suspended sediment transport over ripples accurately. Adequate formula for entrainment rate on seabed ripples has not been suggested up to the present. Even though Equation(4) was proposed for the entrainment over flat beds, it could be used for the entrainment over rippled beds, if the coefficients involved are to be calibrated in due course.

In oder to describe the sediment movement over ripples, the flow field and the sediment concentration field should be investigated. Making use of existing formulas for entrainment, a numerical modelling approach is tried here.

The ripples are assumed to be long-crested, i.e. two-dimensional vertical, and the three-dimensionality of the seabed forms is beyond the scope of the present paper. It is important to compare model results with laboratory experimental results to evaluate the model applicability. A new numerical model system is proposed here, and compared with laboratory measurements. The flow and sediment models of finite difference methods are described in Sections 2.1, and 2.2 respectively. The model application results are described in Section 3.

## 2. FLOW AND SEDIMENT TRANSPORT MODEL

### 2.1. Flow model

The flow model(2DVF-94) used by Kim et al.(1994) is adopted here to simulate flow fields over ripples for waves. Kim et al.'s(1994) model was based on the Marker-and-Cell (MAC) method developed by Welch et al. (1966), and the simplified Marker-and-Cell (SMAC) method by Amsden and Harlow(1970), and Hirt et al.(1975). Hirt et al.'s(1975) model(SOLA) solves the continuity equation and the momentum equations for the two velocity components in the x, z directions and the pressure distribution, that is:

$$\frac{\partial u}{\partial x} + \frac{\partial w}{\partial z} = 0 \quad (5)$$

$$\frac{\partial u}{\partial t} + u\frac{\partial u}{\partial x} + w\frac{\partial u}{\partial z} = -\frac{1}{\rho}\frac{\partial p}{\partial x} + \frac{1}{\rho}\frac{\partial \tau}{\partial z} \quad (6)$$

$$\frac{\partial w}{\partial t} + u\frac{\partial w}{\partial x} + w\frac{\partial w}{\partial z} = -g - \frac{1}{\rho}\frac{\partial p}{\partial z} + \frac{1}{\rho}\frac{\partial \tau}{\partial x} \quad (7)$$

where $x$ is the horizontal coordinate; $z$ is the

vertical coordinate; $u$, $w$ are the turbulence-period-average fluid particle velocities in the $x$ and $z$ directions, respectively; $t$ is time; $\rho$ is the fluid density; $p$ is the pressure; and $\tau$ is the shear stress in the $x-z$ plane. In oder to include the effect of turbulence, Kim et al.(1994) expressed the shear stress term by the mean velocity gradients involving the eddy viscosity concept in 2DVF-94, that is:

$$\frac{\tau}{\rho} = \nu_t\left(\frac{\partial u}{\partial z} + \frac{\partial w}{\partial x}\right) \tag{8}$$

where $\nu_t$ is the eddy viscosity. The eddy viscosity was then modelled using a mixing length hypothesis, that is:

$$\nu_t = l_m^2 \left| \frac{\partial u}{\partial z} + \frac{\partial w}{\partial x} \right| \tag{9}$$

where $l_m$ is the mixing length. The mixing length was assumed to be proportional to the nearest distance to the solid boundary line from the point of interest. When $u$, $w$ and $p$ are calculated from Equations (6) and (7), the velocities $u$ and $w$ do not perfectly satisfy Equation (5). Therefore, an adjustment step is required to obtain $u$, $w$, and $p$ solutions at every time step. In this procedure a convergence parameter, $\varepsilon$ is needed for judgement of the convergence of the iteration. The parameter should be of an order of $10^{-3}$ or smaller, see Hirt et al.(1975). In the present work, a value of $10^{-3}$ is assigned to the parameter for effective calculation. The above convergence parameter produces no much difference, if it lies under a certain value. However, the parameter in the solution need not be smaller than the real fluid compressibility in theory. Another parameter, $\alpha$, which represents the desired amount of upstream differencing between 0.0 and 1.0, is chosen as 1.0 (full upstream) for stable calculation of the advective acceleration of fluid. The value of the parameter affects the solution due to the inherent numerical diffusion. However, since the present application case are for turbulent flows, the numerical diffusion may be included in the turbulence diffusion of larger oder, so that the solutions are not sensitive to the parameter value.

The equations can be solved with appropriate initial and boundary conditions. Since the final solution is obtained after repetition of several number of wave periods, an arbitrary initial condition can be supplied. In the present applications, the uniformly distributed horizontal velocity profiles through the water depth were provided for the initial condition. At the side boundaries, condition of ripple length periodicity is used. Therefore, $u$, $w$ and $p$ at the left side boundary line are exactly the same at the right side boundary line at any time. The driving force of the model is the pressure gradient in the x direction. The force is provided by a sinusoidal curve which produces the sinusoidal variation of the horizontal velocity within a wave period. The model runs for several number of wave periods. When the solution at each wave period dose not change so much as 1 % at every grid point and at every time step in a wave period, the solution at the final wave period is selected as the final solution. In the present simulations, the final solutions were obtained after 5 wave periods. Numerical schemes for the above governing equations and boundary conditions have been proposed by Kim et al.(1994). The present model is applied to a Deltaflume experimental case with an appropriate model grid.

The spacial increments $\Delta x$, $\Delta y$ were selected to be 0.81 cm in oder to resolve the ripple shape and the vortex formation around the ripple. The time increment $\Delta t$ was obtained to satisfy the CFL condition, and was further reduced to 5/800 seconds to secure the stability which is affected by the nonlinear

advection terms in the governing equations. At the top boundary, a no vertical flux condition is applied, which is close to the water tunnel experimental condition.

### 2.2. Suspended sediment Transport Model

A new sediment transport model is set up to simulate the suspended sediment movement over ripples. The governing equation of the suspended sediment transport model is the advection-diffusion equation based on the mass conservation of the suspended sediment, that is:

$$\frac{\partial c}{\partial t}+u\frac{\partial c}{\partial x}+(w-w_f)\frac{\partial c}{\partial z}=\varepsilon_x\frac{\partial^2 c}{\partial x^2}+\varepsilon_z\frac{\partial^2 c}{\partial z^2}+S \tag{10}$$

where $c$ is the instantaneous suspended sediment concentration; $\varepsilon_x$ and $\varepsilon_z$ are the diffusion coefficients in the $x$ and $z$ directions, respectively; and $S$ is the additional source of suspended sediment.

The flow velocities, $u$ and $w$ are obtained from the flow model of the previous section. The diffusion coefficients of the suspended sediment are assumed to be identical to the flow eddy viscosity, and the eddy viscosity is assumed to be isotropic.

The calculation domain is bounded by the upper boundary, the bed boundary, and the two side boundaries. The source or sink occurs at the solid boundary only, where the source represents the entrainment of sediment from the bed, and the sink means the settling of sediment particles from the water column to the bed. The entainment and free settling have often been expressed by the equilibrium condition based on the assumption of quasi-steady flow condition. However, the gradient of concentration becomes less accurate at the bed, when the entrainment rate is low. Therefore, an unsteady expression is adopted for the present work. At the bed boundary the diffusion terms are ignored, and the sediment particles are considered to settle down simply.

The entrainment of sediment from the bed surface (fluid/solid boundary) is now allowed from the whole ripple surface here. Equation (4) is adopted to calculate the sediment entrainment rate on the ripple surface, even though the equation was originally developed for the entrainment over flat beds. The shear stress at a ripple surface point is calculated from the fluid velocities around the grid point, and the roughness at the ripple surface, assuming logarithmic velocity profile as follows:

$$u_* = \varkappa u/\ln(z/z_0) \tag{11}$$

where $u_*$ is the friction velocity($=\sqrt{\tau/\rho}$), $u$ is the horizontal fluid velocity at level $z$, $z_0$ is one thirtieth of the bed roughness, and $\varkappa$ is the Karman constant.

The entrained sediments should be released into the water column. The releasing level of sediment particles is selected at the center of the first grid over solid boundary grid for computational convenience here. Then the released sediments diffuse on both sides (upward and downward) from the level, and convect with the fluid particles and settle down through the fluid simultaneously.

At the side boundary which has a stair shape, the horizontal diffusion through the wall is not allowed.

The governing equation of the suspended sediment movement is transformed into the

$$\frac{c_{i,k}^{n+1}-c_{i,k}^{n}}{\Delta t}+\overline{u}_{i,k}^{\,n}\frac{c_{i+1,k}^{n}-c_{i,k}^{n}}{\Delta x}+(\overline{w}_{i,k}^{\,n}-w_f)\frac{c_{i,k+1}^{n}-c_{i,k}^{n}}{\Delta z}$$
$$=\varepsilon_{x,i,k}^{n}\frac{c_{i+1,k}^{n}-2c_{i,k}^{n}+c_{i-1,k}^{n}}{\Delta x^2}+\varepsilon_{z,i,k}^{n}\frac{c_{i,k+1}^{n}-2c_{i,k}^{n}+c_{i,k-1}^{n}}{\Delta z^2}+S_{i,k}^{n} \tag{12}$$

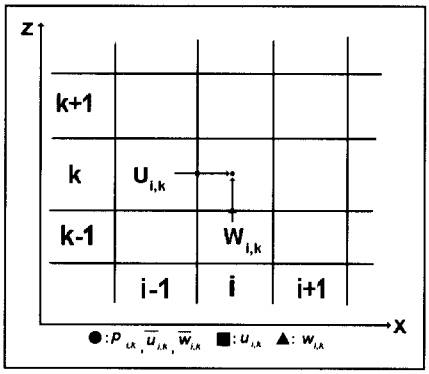


Fig. 1. Variable numbering.

following finite difference equation:

where subscripts $i$ and $k$ are the indices for numbering grid point in the $x$ and $z$ directions, respectively; superscript $n$ is the index for numbering time step; $u$ and $w$ are the velocity components defined at the grid centre in the $x$ and $z$ directions, respectively; $\Delta t$ is the time increment; and $\Delta x$ and $\Delta z$ are the spacial increments. The above difference equation is split into three sub-equations, and solved iteratively, see Kim(1993).

The regular rectangular grid for flow model is again used for the present sediment transport model. The variables are defined as in Fig. 1.

## 3. RESULTS

eltaflume facility at Delft Hydraulics, the

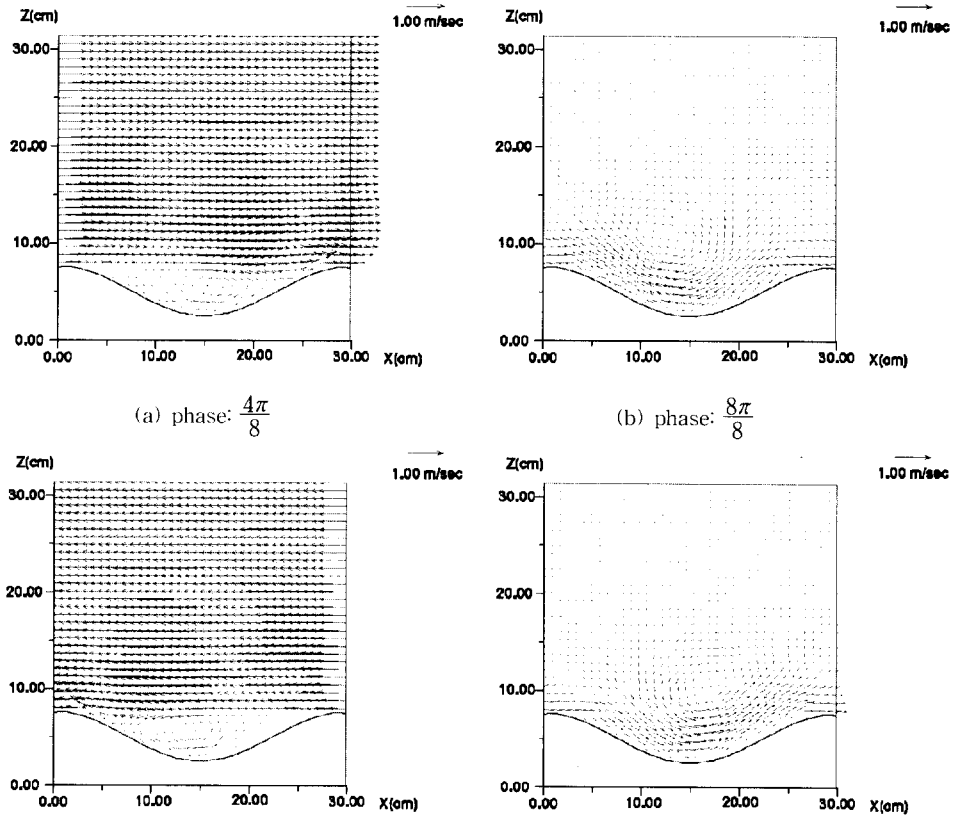


(a) phase: $\frac{4\pi}{8}$

(b) phase: $\frac{8\pi}{8}$

(c) phase: $\frac{12\pi}{8}$

(d) phase: $\frac{16\pi}{8}$

Fig. 2. Calculated flow fields

Netherlands during July and August 1997, see Williams et al.(1998). The length, width, and depth of the flume are 230 m, 5 m, and 7 m, respectively. The Sediment Transport And Boundary Layer Equipment(STABLE) field instrument was used to measure bed sediment response to hydrodynamic forcing in marine conditions. It measured fluid motion using electromagnetic current meters, and suspended sediment concentration using a pump sampler. The median grain size of the experiment( $d_{50}$ ) was 0.329 mm, the wave height(H) was 1.299 m, the wave period(T) was 5.00 s, the water depth(h) was 4.5 m, the ripple height(△) was 0.29 m, and the ripple length( $\lambda$ ) was 0.048 m. The $\Delta x$, $\Delta y$ and $\Delta t$ were chosen as 0.805 cm and 0.00416 sec respectively.

The calculated flow fields for several wave phases are shown in Fig. 2. Strong vortices of the ripple length scale are developed at flow reversals. The general pattern of the computed flow field looks reasonable. The model results show that vortices are generated at the ripple lees, and separated at flow reversal. In general, the computation results show similar flow pattern to the visual observation during the experiment. In order to examine the characteristics of the wave boundary layer flows in detail, the calculated horizontal velocity profiles on ripple crest and trough are compared with that of O'Connor *et al.*'s(1992) one-dimensional vertical(1DV) model results. In general, the computation results show similar flow pattern to the visual observation at flow reversals.

The boundary flow profile shows the

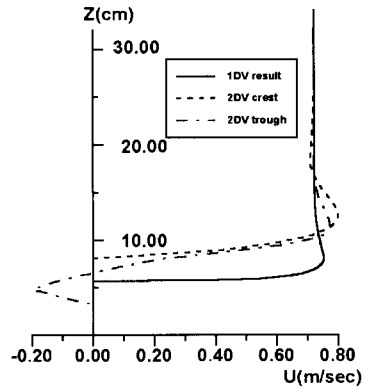


Fig. 3. Horizontal velocity profiles calculated from 1DV and 2DV models.

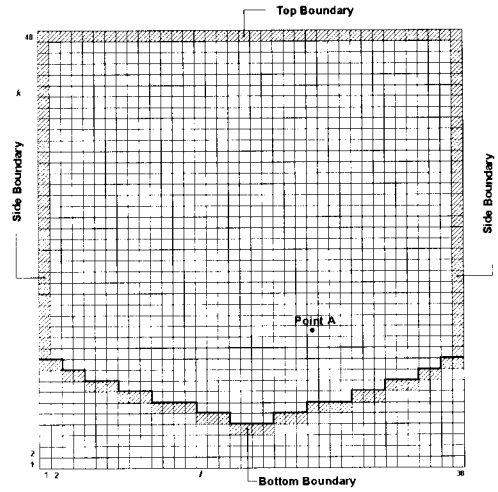


Fig. 4.1. Grid system and Compared Point

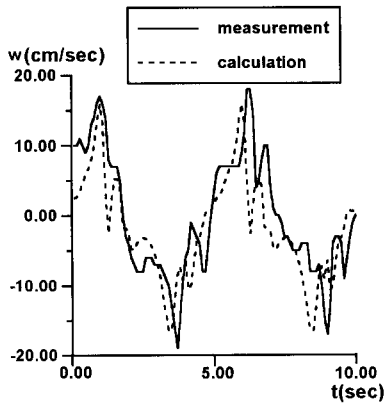


Fig. 4.2. Calculated and measured vertical velocities

overshooting around the top of the boundary layer, see Fig. 3. The 1DV model results are plotted on the traditional vertical scale based on the description of the logarithmic velocity profile, where the origin of z axis has been a mean level of the bed surface. The present experimental results imply that the origin should be modified when the beds are rippled and wave periods are short. Similar wave boundary layer thicknesses are seen in the 2DV and 1DV models results.

The calculated vertical velocity components of the near bed flows at point A in Fig. 4.1 are compared with measured vertical velocity components, see Fig. 4. In Fig. 4, the measurement line represents the ensemble average values obtained from several number of wave periods during the experiments. The averaged values for one wave period are shown in Fig. 4. Both the measurements and calculation results show the effect of vortex movement on the vertical velocity component, so that the velocity variation involves non-sinusoidal components. The calculated vorticity field for four wave phases are shown in Fig. 5, where the plus sign is for the counter-clockwise vorticity. The model results show that strong vortices are produced at flow

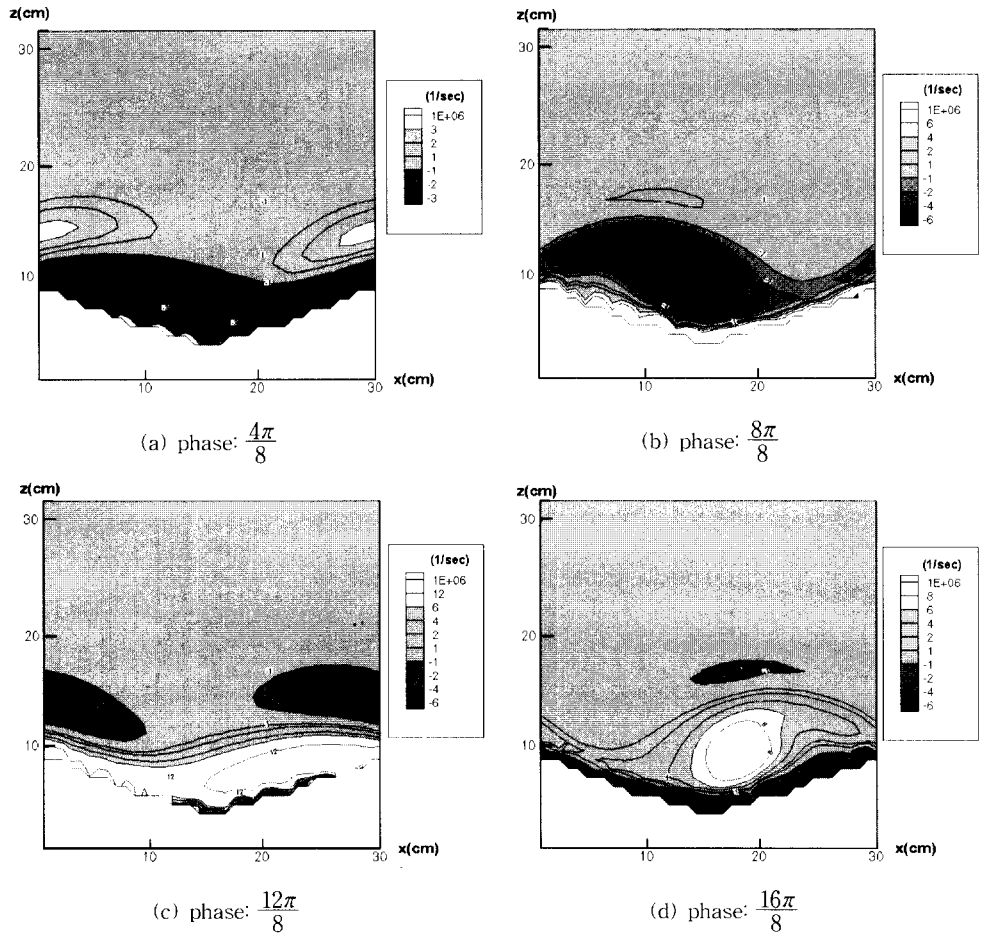


(a) phase: $\frac{4\pi}{8}$

(b) phase: $\frac{8\pi}{8}$

(c) phase: $\frac{12\pi}{8}$

(d) phase: $\frac{16\pi}{8}$

**Fig. 5. Calculated vorticity field.**

reversal phases, and the vortices are separated from the bed and float up after the flow reversals. The calculated vorticity filed shows strong vorticity region near the bed and separated weak vorticity region, the vortex of which was generated during previous half cycle, and decays as time goes by.

The calculated shear stress and pressure variation at ripple crest and trough are shown in Figs. 6 and 7, while the measured values do not exist. A wide range of shear stress is distributed temporally and spacially on the ripple surface. The variation of shear stress and pressure within a wave period demonstrates well the role of vortex movement over ripples.

The sediment model was then applied to the above experimental condition. The calculated suspended sediment concentration contours at four wave phases are shown in Fig. 8. The model results show that the sediment cloud repeats to spread sediment particles on both sides of the ripple crest.

The calculated and measured ripple-length-average, wave-period-average suspended sediment concentration profiles over ripple are shown in Fig. 9. The calculated concentration profile agrees reasonably well with the measurements at Deltaflume. However, the calculated sediment concentration at a level of

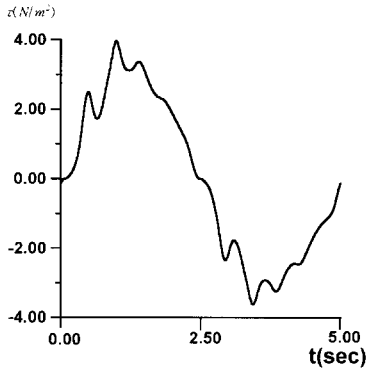


Fig. 6a. Calculated shear stress variation at ripple crest.

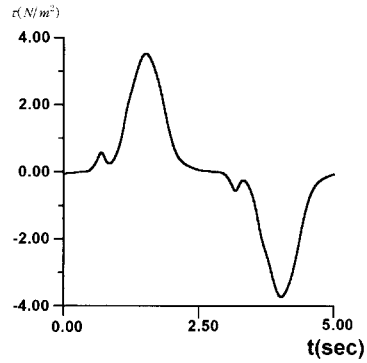


Fig. 6b. Calculated shear stress variation at ripple trough.

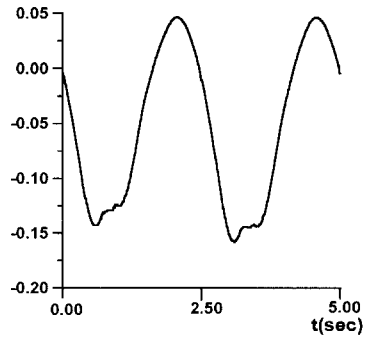


Fig. 7a. Calculated dynamic pressure variation at ripple crest.

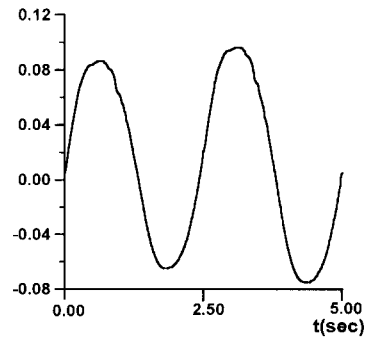


Fig. 7b. Calculated dynamic variation at ripple trough.

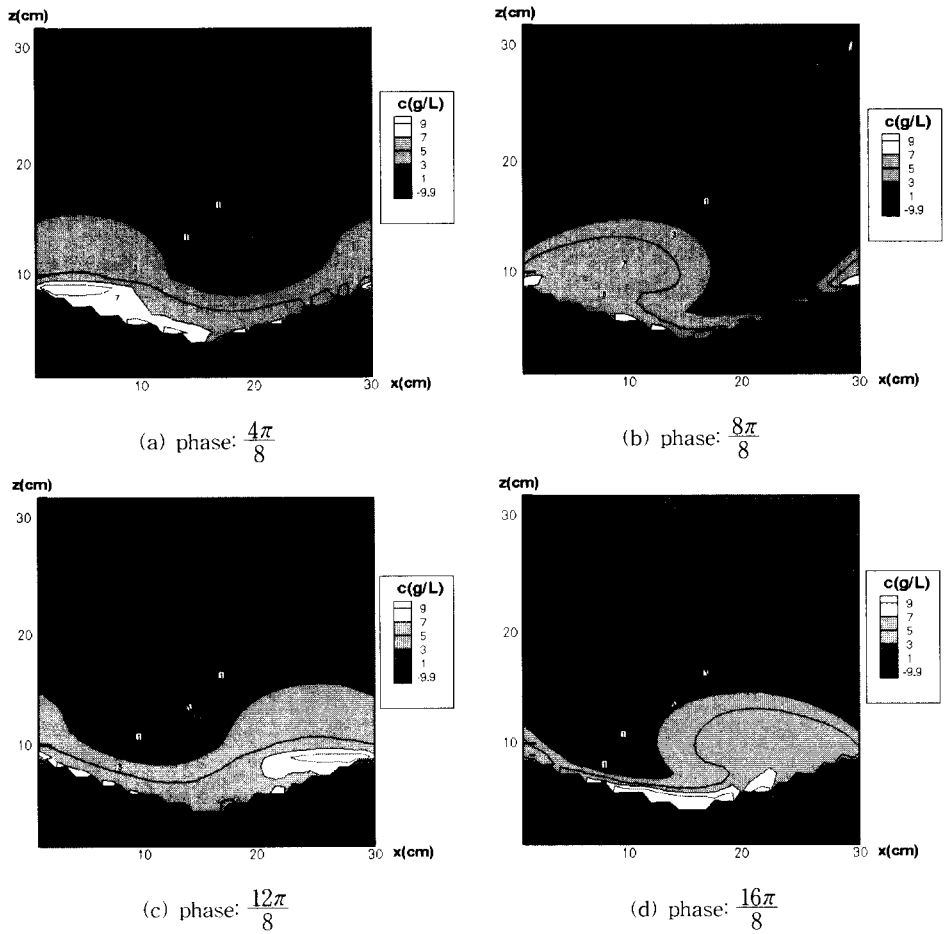


(a) phase: $\frac{4\pi}{8}$

(b) phase: $\frac{8\pi}{8}$

(c) phase: $\frac{12\pi}{8}$

(d) phase: $\frac{16\pi}{8}$

Fig. 8. Calculated suspended sediment concentration field.

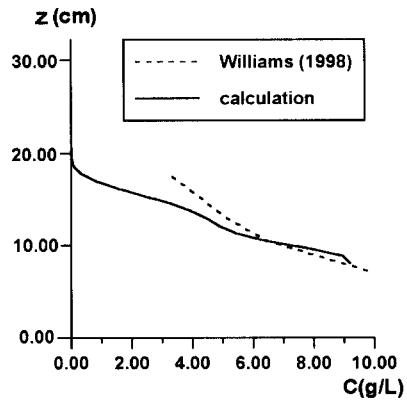


Fig. 9. Calculated and measured suspended sediment concentration profiles.

a few times ripple height shows steep gradient compared to the measurements. This could be explained by the assumption adopted in the modelling procedure the spacial variation of the vertical orbital velocity within a wave length is ignored like the flows in oscillating water tunnel.

The model was then applied to an artificial long-crested random wave case. The significant wave height was selected to be identical to the wave height of the above regular wave experiment, and the peak wave period was selected to be identical to the wave period of the above regular wave experiment.

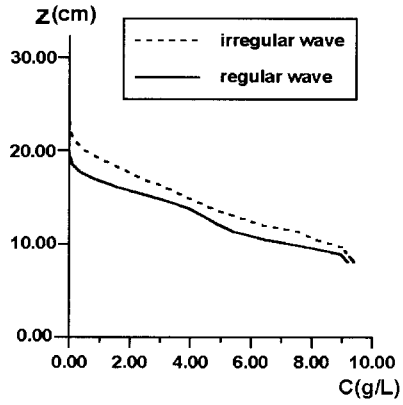


Fig. 10. Predicted suspended sediment concentration for random waves.

The wave spectrum was assumed to be JONSWAP for the numerical simulation. The calculated sediment concentration profile for the random waves is shown in Fig. 10 with that for monochromatic waves. In Fig.10 the near bed suspended sediment concentrations are higher for random waves than those for monochromatic waves due to the nonlinear relationship between wave orbital velocity, bed shear stress, and the entrainment rate from the bed. Fig. 10 also shows that the gradient of suspended sediment concentration over ripples for random waves is smaller than that for monochromatic waves. This may be explained by the diffusion effect due to the groupiness of random waves.

## 4. CONCLUSIONS

The flow and sediment transport over ripples have been described by numerical modelling work in the present paper. The model system is composed of an existing flow model and a new sediment transport model. The calculated vertical velocity variation using the flow model agrees well with the measurements. The sediment transport model solves directly the advection-diffusion equation, and involves sediment entrainment from the whole ripple surface. The calculated suspended sediment profile also agrees reasonably well with the measurements. However, the calculated concentrations at high levels are lower than the measurements. This implies that diffusion coefficients at high levels calculated from the flow model are underestimated.

The model simulated the flow and sediment concentration movement for long-crested random waves for comparison with that for monochromatic waves of the significant wave height and the peak period. The calculated wave-period-average sediment concentrations for random waves are generally higher than those for regular waves. The predicted upper limit of sediment diffusion for random waves is also higher than that for monochromatic waves. The model simulation results for random waves imply that the representative wave height and wave period should be carefully chosen. The model could be applied to random wave simulations with experimental results in the future for further verification of the sediment transport model.

## 5. ACKNOWLEDGEMENTS

The present work was supported by the Korea Research Foundation Grant(KRF-95-04-E-0204), the Commission of the European Communities Directorate General for Science and Education, Research and Development under contract number MAS3-CT97-0106, and KISTEP under contact number 99-I-New-05.

## REFERENCES

Amsden, A.A. and Harlow, F.H. (1970). *The SMAC method*, Los Alamos Scientific Laboratory, Report LA-4370.

Bagnold, R.A. (1946). "Motion of waves in shallow water. Interaction between waves and sand bottoms." *Proc. Roy. Soc.* A187, pp. 1-15.

Blondeaux, P. and Vittori, G. (1990).

"Oscillatory flow and sediment motion over a rippled bed." *International Conference on Coastal Engineering*, ASCE, pp. 2186-2199.

Bosman, J.J. (1982). *Concentration measurements under oscillatory motion.* DH Report M 1695, Part II.

Du Toit, C.G. and Sleath, J.F.A. (1981). "Velocity measurement close to rippled beds in oscillatory flow. *Journal of Fluid Mechanics.*" Vol. 112, pp. 71-96.

Hansen, E.A., Fredsoe, J. and Deigaard, R. (1991). Distribution of suspended sediment over wave generated ripples. *International Symposium on the Transport of Suspended Sediments and its Mathematical Modelling*, Florence, Italy, pp. 111-128.

Huynh-Thanh, S. and Temperville, A. (1990). "A numerical model of the rough turbulent boundary layer in combined wave and current interaction." *International Conference on Coastal Engineering*, ASCE, pp. 853-866.

Kim, Hyoseob., B.A. O'Connor, Y. Shim. (1994). "Numerical modelling of flow over ripples using SOLA method." *24th International Conference on Coastal Engineering*, ASCE, pp. 2140-2154

Kim, Hyoseob. (1993). Three dimensional sediment transport model. Ph.D. Thesis, University of Liverpool, Liverpool, UK.

Longuet-Higgins, M.S. (1981). "Oscillating flow over steep sand ripples." *Journal of Fluid Mechanics*, Vol. 107, pp. 1-35.

MacPherson, B. (1984). Flow and sediment transport over steep sand ripples. Ph.D. Thesis, The University of Cambridge, UK.

Nielsen, P. (1992). *Coastal bottom boundary layers and sediment transport.* World Scientific.

O'Connor, B.A., Harris, J., Kim, H., Wong, Y.K., Oebius, H.U., and Williams, J.J. (1992). "Bed boundary layers." *International Conference on Coastal Engineering*, ASCE, pp. 2307-2320.

O'Connor, B.A. (1998). *Inlet Dynamics Initiative; Algarve(INDIA)*, University of Liverpool, End of-Year(12 Monthly) Report.

Sato, S. (1987). Oscillatory boundary layer flow and sand movement over ripples. Ph.D. Thesis, The University of Tokyo, Japan.

Tsujimoto, G., Hayakawa, N., Ichiyama, M., Fukushima, Y. and Nakamura, Y. (1991). "A study on suspended sediment concentration and sediment transport mechanism over rippled sand bed using a turbulence model." *Coastal Engineering Japan*, Vol. 34, No. 2, pp. 177-189.

Van Rijn, L.C. (1989). *Handbook sediment transfort by currents and waves.* Report H 461, Delft Hydraulics.

Welch, J.E., Harlow, F.H., Shannon, J.P. and Daly, B.J. (1966). *The MAC method*, Los Alamos Scientific Laboratory, Report LA-3425.

Williams, J.J., Bell, P.S., Coates, L.E., Hardcastle, P.J., Humphery. J.D., Moores, S.P., Thorne, P.D., Trouw, K. (1998). *Evaluation of field equipment used studies of sediment dynamics*, Proudman Oceanographic Laboratory, Report 53.

(논문번호:99-062/접수:1999.08.19/심사완료:1999.12.28)